Journal of Molecular Liquids 222 (2016) 435–440

Contents lists available at ScienceDirect

Journal of Molecular Liquids

journal homepage: www.elsevier.com/locate/molliq

Cu_2ZnI_4/ZnO nanocomposites: In-situ synthesis, characterization and optical properties

Fariba Razi, Faezeh Soofivand, Masoud Salavati-Niasari *

Institute of Nano Science and Nano Technology, University of Kashan, Kashan, P. O. Box. 87317-51167, Islamic Republic of Iran

ARTICLE INFO

Article history:
Received 8 June 2016
Received in revised form 16 July 2016
Accepted 18 July 2016
Available online 20 July 2016

Keywords:
Cu_2ZnI_4
Superionic conductors
Thermal-treatment
Photocatalyst
Nanocomposite

ABSTRACT

In this work, copper zinc tetraiodide/zinc oxide (Cu_2ZnI_4/ZnO) nanocomposites were successfully synthesized by simple solid-state method. The effect of various parameters such as Cu^+/Zn^{+2} molar ratio, time and temperature of reaction on morphology, size and purity of products was investigated. The as-prepared products were characterized by X-ray diffraction (XRD), field emission scanning and transmittance electron microscopy (FESEM, TEM), and X-ray energy dispersive spectroscopy (EDS) analysis. Application of Cu_2ZnI_4/ZnO nanocomposite as photocatalyst was confirmed by the band gap estimated through UV–vis spectroscopy. To investigate the photocatalytic properties of this product, photooxidation of methyl orange (MO) was performed. The photocatalytic test shows that the methyl orange degradation was about 54.2% under UV irradiation for 90 min.

1. Introduction

Nanomaterials have unique properties and many applications in various fields, so the scientists have focused on investigation of these materials. Nowadays, nanotechnology has considered as a manufacturing engineering that can be used to form materials with desired properties. Nanotechnology has been defined as the design, characterization, production, and application of structures, devices and systems by controlling shape and size at nanometer scale [1] and preparation of new compounds such as: nanocomposites and multi-component compounds [2–4]. Composites are compounds that are made from two or more constituent that their characteristics are different from the individual components. Material scientists and engineers have attracted much attention to nanocomposites due to their fascinating properties. Nanocomposites demonstrate good advantages over conventional materials and have many applications in various fields [5–7]. M_2NI_4 compounds are examples of multi-component compounds that are classified in two groups: smart materials and superionic conductors [8–10].

Smart materials are compounds that can respond to environmental changes and its one or more properties can be changed. These materials can be called by type of environmental stimuli and its response to related stimuli, so there are different types of smart materials such as shape-memory alloy, piezoelectric, and chromic materials [11]. Chromic compounds have various sub-sets such as: photochromic, thermochromic and piezochromic compounds. Stimuli of these compounds can be light, temperature, change of applied pressure, but all of their response is color change, reversibly [12]. Recently, superior attention is fascinated to thermochromic compounds because of their commercial applications and their role in improving temperature indicators and recording devices. On the other hand, M_2HgI_4 compounds ($M = 1/2\ Pb^{+2}$, Ag^+, Cu^+) are a class of thermochromic materials that their phase and color change at a certain temperature [13]. Changing phase cause to change ionic conductivity in these compounds, on the other word, these compounds can be classified in superionic conductors that exhibit exceptionally high values of ionic conductivity within the solid state [14]. Superionic compounds are solid state fast ion conductors that can be used as solid-state electrolytes in solid-state batteries, solar and fuel cells. The structure of these compounds before temperature of the phase transition is as follows: the iodide form a face-centered cubic (fcc) lattice that 75% of its tetrahedral sites are occupied by two one-valance cations and one two-valance cation and 25% of its tetrahedral sites remain empty, but at above phase transition temperature three cations are disturbed among the four tetrahedral sites provided by the fcc sub-lattice of the iodide, randomly [15].

The M_2NI_4 compounds, which $M = Ag^+$, Cu^+, $N = Cd^{+2}$, Hg^{+2}, Pb^{+2} have been widely studied [13–16], but the studies on Cu_2ZnI_4 is less. In this work, Cu_2ZnI_4/ZnO nanocomposite was prepared by a simple thermal-treatment method. The effect of various parameters such as molar ratio of Cu^+ to Zn^{+2}, temperature and time reaction on purity, morphology, size, and size distribution of products were investigated.

* Corresponding author.
E-mail address: Salavati@kashanu.ac.ir (M. Salavati-Niasari).

http://dx.doi.org/10.1016/j.molliq.2016.07.078
0167-7322/

The obtained products were characterized by X-ray diffraction (XRD), scanning and transmittance electron microscopy (SEM, TEM), and X-ray energy dispersive spectroscopy (EDS) analysis.

2. Experimental

All the chemicals reagents used in our experiments were of analytical grade and were used as received without further purification. $Zn(NO_3)_2 \cdot 6H_2O$, $CuSO_4 \cdot 5H_2O$, $NaHSO_3$, and $LiI \cdot 2H_2O$ were purchased from Merck. GC-2550TG (Teif Gostar Faraz Company, Iran) were used for all chemical analyses. The XRD of products was recorded by a Rigaku D-max C III XRD using Ni-filtered Cu Kα radiation. SEM images were obtained on Philips XL-30ESEM equipped with an energy dispersive X-ray spectroscopy. The EDS analysis with 20 kV accelerated voltage was done.

At the first, tan precipitation of CuI was prepared from 0.1 g $CuSO_4 \cdot 5H_2O$, 0.1 g $NaHSO_3$ and 0.07 g $LiI \cdot 2H_2O$ in 75 ml of distilled water. Then, white precipitation of ZnI_2 was formed from $Zn(NO_3)_2 \cdot 6H_2O$ with stoichiometric amount from $LiI \cdot 2H_2O$ (by considering the molar ratio of Cu^+ to Zn^{+2} in various experiments; the amounts of $Zn(NO_3)_2 \cdot 6H_2O$ to prepare ZnI_2 was changed from 0.07 g to 0.05 g). Finally, CuI was added to ZnI_2, and then the mixture was grinded and was heated to 160, 180, and 200 °C for 24, 18, and 12 h in different experiments. The various experiments were applied to find the optimum condition; details of experiments were illustrated in Table 1.

3. Results and discussion

Fig. 1(a)–(c) illustrates SEM images of samples 1–3, respectively. The fine and isolated particles and some of the aggregated structures are related to sample 1 (Fig. 1(a). SEM of sample 2 was given in Fig. 1(b), a homogenous and dense basis that filled by different structures such as capsule-like and particles are shown. In Fig. 1(c) that depicts SEM image of sample 3, agglomerated nanoparticles with average size about 50 nm together 100 nm-sized capsule-like nanostructures are shown.

XRD analysis, which is the most useful technique for identification of crystalline structure, was employed to investigate the prepared samples. In Fig. 1(a)–(c), the XRD patterns of samples 1–3 are shown. The diffraction lines of these patterns are attributed to Cu_2ZnI_4 (JCPDS = 40-1169) and ZnO (80-0075) phases. The formation of ZnO as a second phase can be explained by a proposed mechanism as follows: ZnI_2 readily absorbs water from the atmosphere and transforms to $Zn(OH)_2$. On the other side, $Zn(OH)_2$ can be transformed to ZnO through thermal treatment at temperature above 150 °C, so $Zn(OH)_2$ is considered as an intermediate in this reaction [17]. The intensity of diffraction lines of ZnO (in samples 1–3 as follows: $1 < 3 < 2$ that can be connected to the molar ratio of Cu^+ to Zn^{+2} in these samples). The proposed mechanism for formation of products:

$$Cu(SO_4)_2 \cdot 5H_2O + LiI \cdot 2H_2O + NaHSO_3 \rightarrow CuI + \text{By-products}$$

$$Zn(NO_3)_2 \cdot 5H_2O + LiI \cdot 2H_2O \rightarrow ZnI_2 + LiNO_3$$

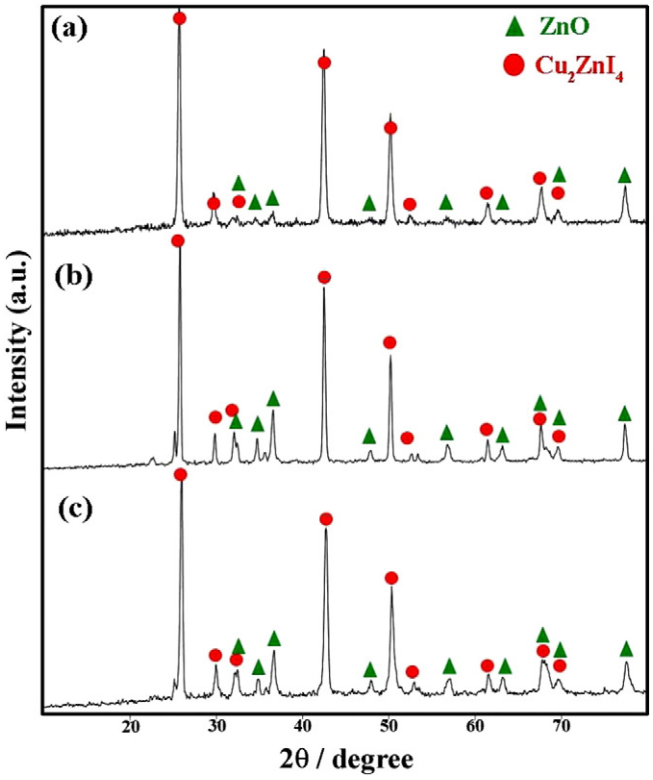

Fig. 1. XRD patterns of sample no. (a) 1, (b) 2, and (c) 3.

$$CuI + ZnI_2 \rightarrow Cu_2ZnI_4$$

$$ZnI_2 \xrightarrow[\text{Absorb water from atmosphere}]{} Zn(OH)_2 \text{ (Intermediate product)} \xrightarrow[\text{Thermal-treatment; temperature} > 150\ ^oC]{} ZnO$$

The effect of the ratio of Cu^+:Zn^{+2} on the morphology and size of the products (samples 1–3) was investigated (in three ratios of 1, 0.5, and 2 for sample 1–3, respectively). In Fig. 2(a), the SEM image shows that sample 1 obtained with the molar ratio of $Cu^+/Zn^{+2} = 1$, consists of some structures with average size 100 nm and nanoparticles with diameters about 40 nm. The SEM image of sample 2 is shown in Fig. 2(b), this image consists of a homogenous and dense basis that filled with different structures such as micrometer-sized capsule-like and particles with various sizes are shown. The SEM images in Fig. 2(c) shows that sample 3, consists of capsule-like structure with average width 100 nm and length 300 nm, and the aggregated particles with diameters about 60 nm.

For studying the formed phases of sample 4 and 5, the XRD patterns of these samples are given in Fig. 3(a) and (b). In Fig. 3(a), the diffraction lines are related to three phases of Cu_2ZnI_4 (JCPDS = 40-1169), $Zn(OH)_2$ (JCPDS = 41-1359), mainly and ZnO (80-0075) partially. $Zn(OH)_2$ can be considered as an intermediate of transformation reaction of ZnI_2 to

Table 1
The preparation conditions of sample no. 1–7.

Sample no.	Cu^+:Zn^{+2} molar ratio	Temperature of reaction (°C)	Time of reaction (h)	The prepared products
1	1: 1	200	24	ZnO, Cu_2ZnI_4
2	1: 2	200	24	ZnO, Cu_2ZnI_4
3	2: 1	200	24	ZnO, Cu_2ZnI_4
4	1: 1	200	18	ZnO, $Zn(OH)_2$, Cu_2ZnI_4
5	1: 1	200	12	ZnO, $Zn(OH)_2$, Cu_2ZnI_4
6	1: 1	180	24	ZnO, $Zn(OH)_2$, Cu_2ZnI_4
7	1: 1	160	24	ZnO, $Zn(OH)_2$, Cu_2ZnI_4

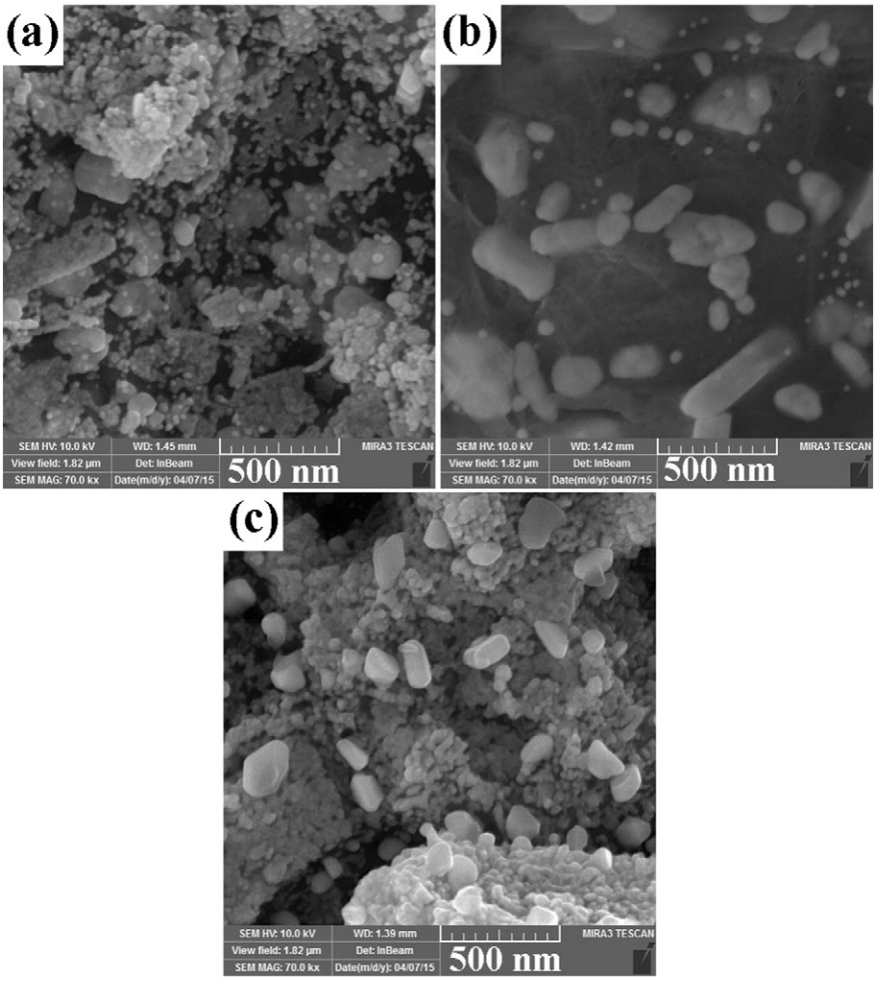

Fig. 2. SEM images of sample no. (a) 1, (b) 2, and (c) 3.

ZnO at a temperature about 200 °C. The presence of $Zn(OH)_2$ in samples 4, 5 and its absence in samples 1–3 can be related to the enough time for transformation of $Zn(OH)_2$ to ZnO, so the presence of $Zn(OH)_2$ as intermediate product of this reaction (transformation of ZnI_2 to ZnO) is justified.

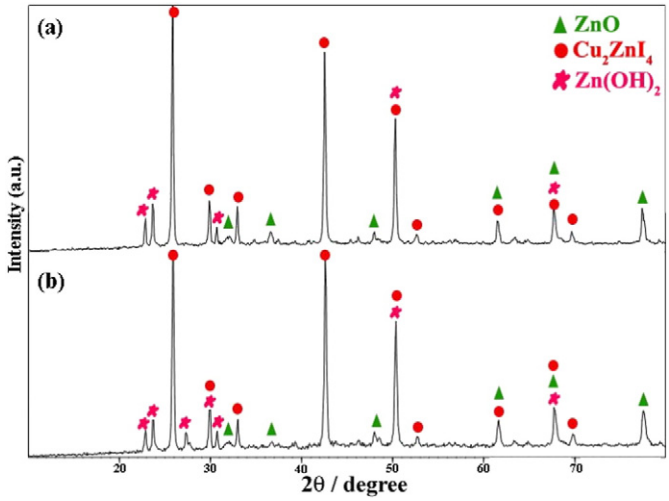

Fig. 3. XRD patterns of sample no. (a) 4, (b) 5.

Next, the effect of time reaction was investigated and experiments were done at two other times 18, and 12 h. The SEM images of these products are shown in Fig. 4(a) and (b). In Fig. 4(a), the irregular and heterogeneous structures are shown that related to sample 4. SEM image of sample 5 is illustrated in Fig. 4(b), this image consists of nano-sized particles and capsules-like.

The XRD patterns of sample 6, 7 were given in Fig. 5(a) and (b), these patterns consist of three phases Cu_2ZnI_4 (JCPDS = 40-1169), $Zn(OH)_2$ (JCPDS = 41-1359), and ZnO (JCPDS = 80-0075). As said above, the presence of $Zn(OH)_2$ as an intermediate in these patterns is due to the low temperature of reaction. So $Zn(OH)_2$ cannot be transformed to ZnO, completely and diffraction lines of $Zn(OH)_2$ are shown in these patterns. The crystallinity of sample 7 is lower than sample 6, because of the reaction temperature in sample 6 is lower than sample 7.

In continuation, the effect of temperature on size and morphology of products was investigated; SEM images of samples 6 and 7 are shown in Fig. 6(a) and (b), respectively. In Fig. 6(a), the larger structures are shown that consist of uniform and fine particles with an average size about 20 nm. The agglomerated nanoparticles with size about 100 nm were shown in Fig. 6(b) (sample 7). The SEM image of this sample illustrates an amorphous basis together with other structures.

By considering all of SEM images and XRD patterns of as-prepared samples, sample 1 was chosen as desired sample and further analyses such as EDS, TEM, and UV–vis were applied on this sample, furthermore application of this sample as a photocatalyst was carried out under UV irradiation.

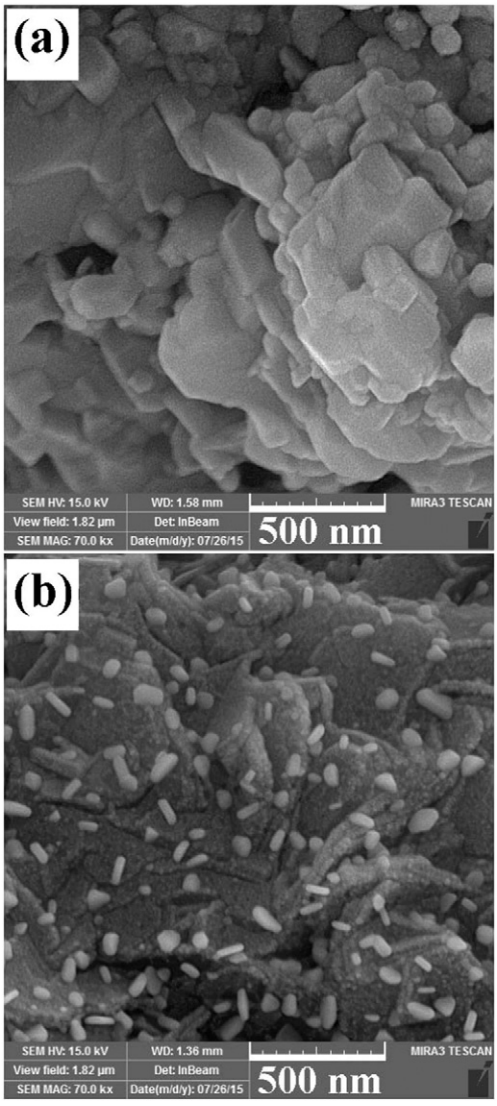

Fig. 4. SEM images of sample no. (a) 4, (b) 5.

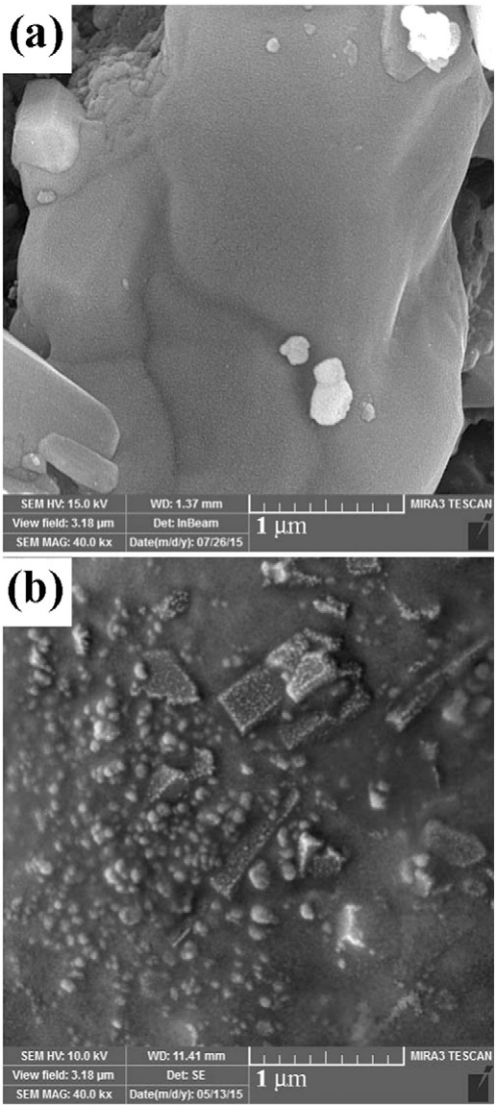

Fig. 6. SEM images of sample no. (a) 6, (b) 7.

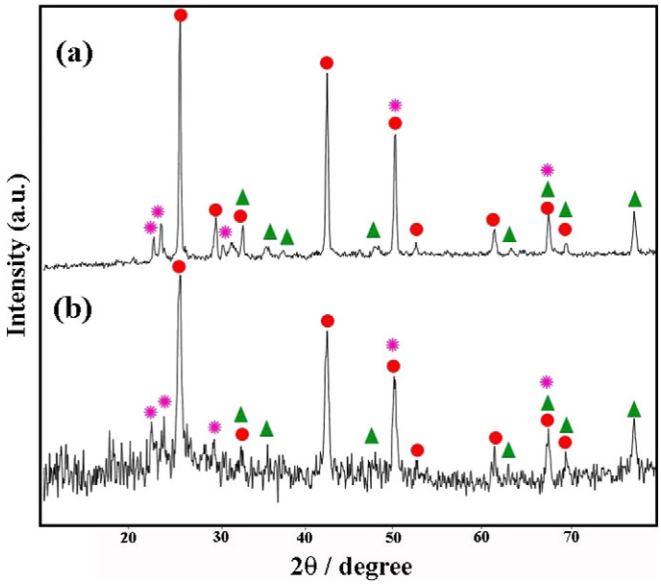

Fig. 5. XRD patterns of sample no. (a) 6, (b) 7.

The TEM images of the as-prepared Cu_2ZnI_4/ZnO nanocomposite are shown in Fig. 7(a), (b), and (c). Fig. 7(a)–(c) depicts TEM images of the as-prepared Cu_2ZnI_4/ZnO nanocomposite (sample no. 1) in various scale 200, 100, and 50 nm, respectively. The average size of these nanoparticles is about 35 nm. To provide typical histograms of the particle diameters, the average particle diameter of the Cu_2ZnI_4/ZnO nanocomposite was estimated by measuring over 40 particles on the TEM images by using Digimizer software. As shown in Fig. 7(d), the particle size distribution of sample 1 is observed in the range of 20–100 nm. By considering the particle size distribution of the sample 1 can be said that the average, minimum and maximum size of particle size are 36.82 nm, 20.99 nm, and 97.33 nm, respectively.

In The EDS spectrum of as-prepared product from sample 1 (Fig. 8), Cu, Zn, and I elements are detectable. The other peaks were not detected in this spectrum, so purity of the as-prepared product was confirmed.

Fig. 9(a) shows the UV–vis absorption spectrum of as-prepared Cu_2ZnI_4/ZnO nanocomposite from sample 1. In this spectrum an absorption peak around approximate 336 nm can be observed. Optical band gap (Eg) may be evaluated based on the optical absorption spectrum using the following equation [18–23]: $(Ah\upsilon)^n = B(h\upsilon - Eg)$; Where

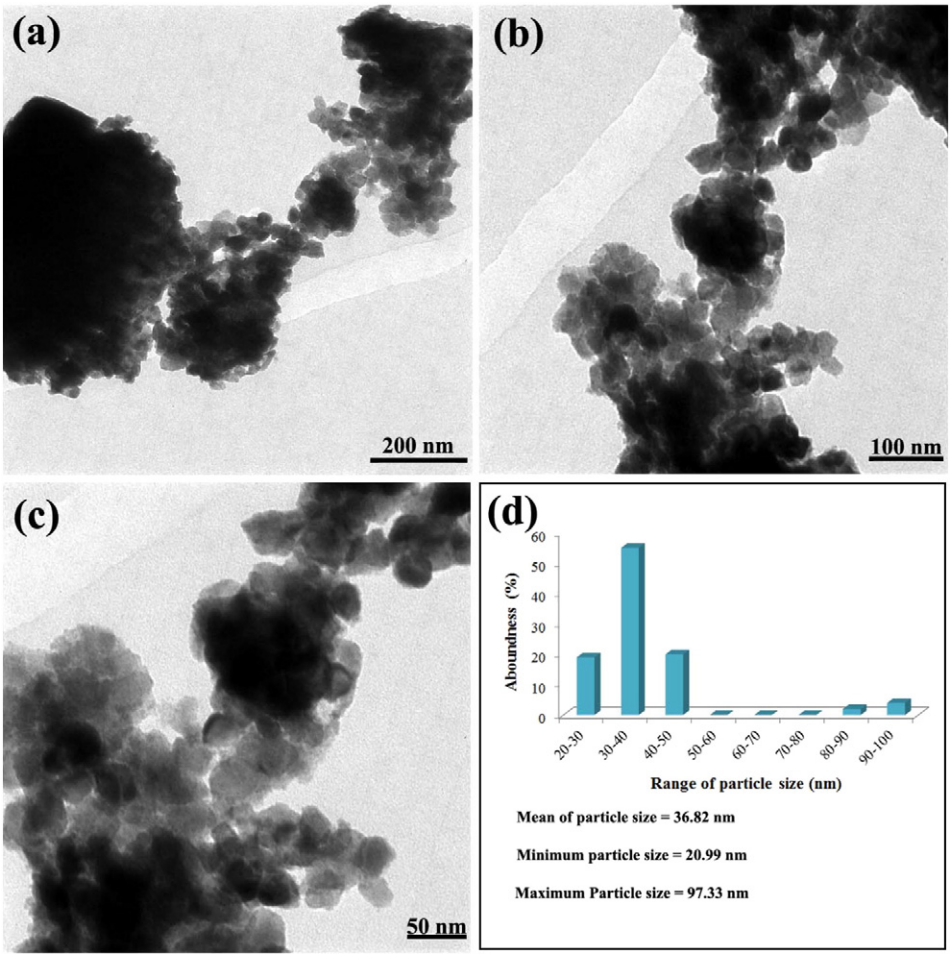

Fig. 7. TEM images of sample no. 1 at scale (a) 200, (b) 100, (c) 50 nm and (d) particle size distribution of sample no. 1.

hυ is the photon energy, A is absorbent, B is a material constant and n is 2 or 1/2 for direct and indirect transitions, respectively. The optical band gap for the absorption peak is obtained by extrapolating the linear portion of the $(Ah\upsilon)^n$ curve versus hυ to zero. No linear relation was found for n = 1/2, suggesting that the prepared Cu_2ZnI_4/ZnO nanocomposite is semiconductor with direct transition at this energy. The band gap of as-prepared Cu_2ZnI_4/ZnO nanocomposite was calculated about 3 eV (Fig. 9(b). The calculated band gap confirms that this compound can be used as an effective photocatalyst.

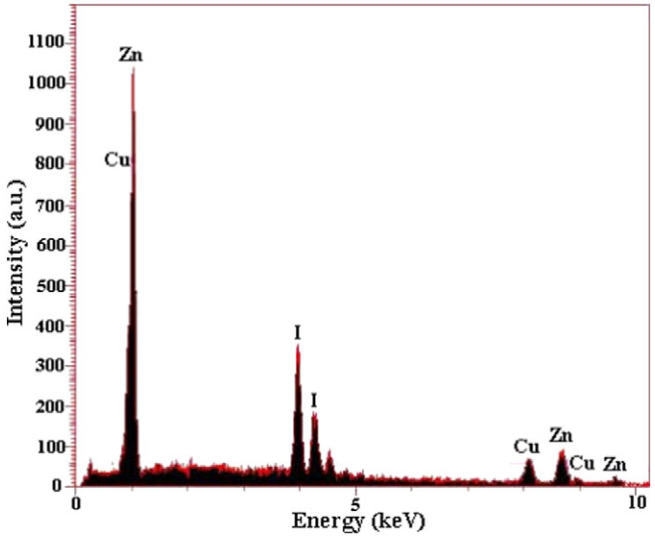

Fig. 8. EDS spectrum of samples no. 1.

The photocatalytic activity of Cu_2ZnI_4/ZnO nanocomposite was investigated by monitoring the degradation of methyl orange (MO) solution dye under UV light irradiation (Fig. 10). The photocatalytic degradation reaction was performed out in a quartz photocatalytic reactor and carried out with a 10 ppm MO solution containing 0.05 g of photocatalyst (Cu_2ZnI_4 nanoparticles). This mixture was aerated for 30 min to reach adsorption equilibrium. Then, the mixture was placed inside the photoreactor in which the vessel was 40 cm away from the UV of 100 W Osram lamp. The quartz vessel and light sources were placed inside a black box equipped with a fan to prevent UV leakage. The experiments were performed at room temperature and pH of the MO solution was adjusted 2–3. The MO degradation percentage was calculated by Eq. (1) as follows:

$$D.P.(t) = (A_0 - A_t)/A_0 \times 100 \quad (1)$$

where A_0 and A_t are the absorbance value of MO solution at 0 and t min, respectively [2].

According to photocatalytic calculations by Eq. (1), the MO degradation percentage was about 54.2% after 90 min irradiation of UV light in presence Cu_2ZnI_4 nanoparticles as photocatalyst.

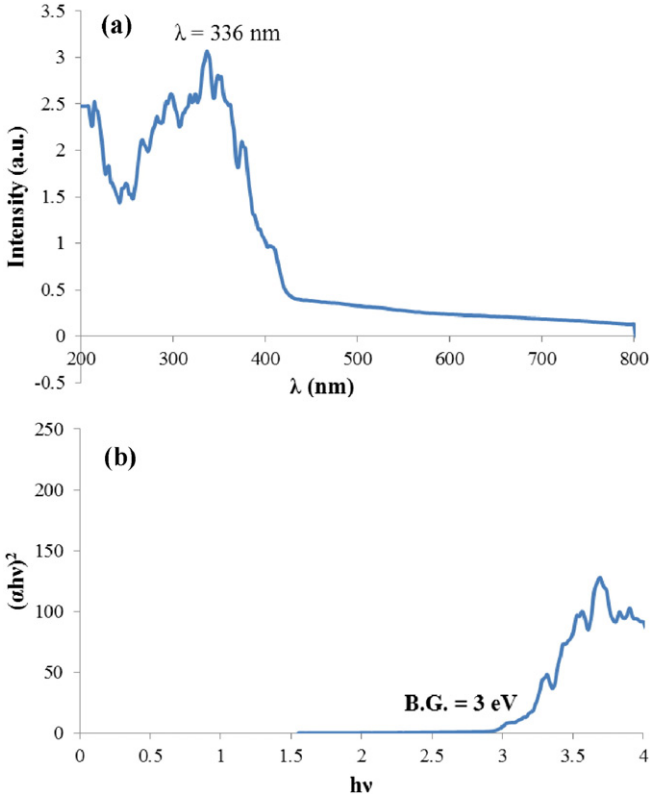

Fig. 9. (a) UV–vis spectrum, (b) curve $(Ah\upsilon)^n$ versus hυ of sample no. 1.

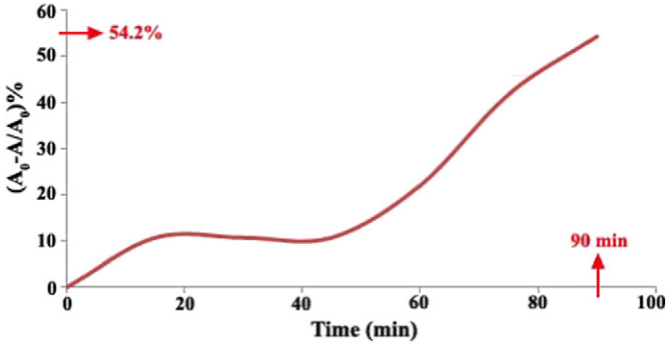

Fig. 10. Degradation of MO under UV irradiation in presence of sample no. 1 as photocatalyst.

4. Conclusions

In this project, we connect three fascinated fields: photocatalytic activity, thermochromic phenomena, and superionic conductivity with the synthesis of Cu_2ZnI_4/ZnO nanocomposite. Herein, Cu_2ZnI_4/ZnO nanocomposite with average size about 35 nm was synthesized by the simple thermal-treatment method. The role of various parameters such as molar ratio of Cu^{+}/Zn^{+2}, time and temperature of the reaction was investigated on purity, size and morphology of products and optimum condition for preparation of Cu_2ZnI_4/ZnO nanocomposite was found. The further analyses were carried out on the product prepared in the desired condition such as TEM, EDS, UV–vis. By considering band gap estimated through UV–vis spectrum of this product, application of Cu_2ZnI_4/ZnO nanocomposite obtained in this work confirms as photocatalyst. To investigate the photocatalytic properties of this product, photo-oxidation of methyl orange (MO) was performed. The photocatalytic test shows that the methyl orange degradation was about 54.2% after 90 min irradiation of UV light.

Acknowledgements

Authors are grateful to the council of Iran National Science Foundation and University of Kashan for supporting this work by Grant No (159271/576).

References

[1] K. Aslan, I. Gryczynski, J. Malicka, E. Matveeva, J.R. Lakowicz, C.D. Geddes, Metal-enhanced fluorescence: an emerging tool in biotechnology, Curr. Opin. Biotechnol. 16 (2005) 55–62.
[2] F. Soofivand, F. Mohandes, M. Salavati-Niasari, Silver chromate and silver dichromate nanostructures: sonochemical synthesis, characterization, and photocatalytic properties, Mater. Res. Bull. 48 (2013) 2084–2094.
[3] S. Alikhanzadeh-Arani, M. Salavati-Niasari, M. Almasi-Kashi, Influence of the utilized precursors on the morphology and properties of YBa 2 Cu 3 O 7 − y superconducting nanostructures, Phys. C 488 (2013) 30–34.
[4] S. Kondo, A. Masaki, T. Saito, H. Asada, Fundamental optical absorption of CsPbI 3 and Cs 4 Pbl 6, Solid State Commun. 124 (2002) 211–214.
[5] M. Masjedi-Arani, M. Salavati-Niasari, A simple solid-state approach for synthesis and characterization of CdO–ZrO2–CdZrO3 nanocomposites, J. Mater. Sci. Mater. Electron. 26 (2015) 2316–2322.
[6] M. Mousavi-Kamazani, M. Salavati-Niasari, A simple microwave approach for synthesis and characterization of Ag 2 S–AgInS 2 nanocomposites, Compos. Part B 56 (2014) 490–496.
[7] F. Soofivand, M. Salavati-Niasari, Co 3 O 4/graphene nanocomposite: pregraphenization synthesis and photocatalytic investigation of various magnetic nanostructures, RSC Adv. 5 (2015) 64346–64353.
[8] K. Siraj, R. Rafiuddin, Electrical conductivity behavior of CdHgI4 – CuI mixed system, Int. J. Chem. 3 (2011) 174–179.
[9] R. Blachnik, U. Stöter, The phase diagram AgI-ZnI2, Thermochim. Acta 145 (1989) 93–99.
[10] R. Ammlung, R.P. Scaringe, J.A. Ibers, D. Shriver, D. Whitmore, Trends in heavy-metal solid state ionic conductors: a comparison of Cu+, Ag+, In+, and Tl+ transport, J. Solid State Chem. 29 (1979) 401–415.
[11] S. Kamila, Introduction, classification and applications of smart materials: an overview, Am. J. Appl. Sci. 10 (2013) 876.
[12] M.A. Chowdhury, M. Joshi, B.S. Butola, J. Eng. Fibers Fabr. 9 (2014) 107.
[13] A. Ahmad, Phase transition study in a [Cu2HgI4: 0·xAgI] mixed composite system, Bull. Mater. Sci. 33 (2010) 419–425.
[14] A. Ahmad, Composition-induced phase transition in a [Ag2HgI4: 0.2 AgI] mixed composite system doped with CuI, Open Chem. 8 (2010) 1227–1235.
[15] N.A. Ahmad, Synthesis, Characterization, Fast Ion Transport and Phase Transition in a [Ag2HgI4: 0.x AgI] Type Superionic Mixed Composite Materials (x = 0.2, 0.4, 0.6 mol·wt.%), 2011.
[16] O. Yunakova, V. Miloslavsky, E. Kovalenko, Absorption spectrum of Cu, Funct. Mater. 10 (2003) 4.
[17] L.E. Greene, B.D. Yuhas, M. Law, D. Zitoun, P. Yang, Solution-grown zinc oxide nanowires, Inorg. Chem. 45 (2006) 7535–7543.
[18] J. Tauc, Optical properties and electronic structure of amorphous Ge and Si, Mater. Res. Bull. 3 (1968) 37–46.
[19] H.R. Momenian, M. Salavati-Niasari, D. Ghanbari, B. Pedram, F. Mozaffar, S. Gholamrezaei, The effect of $Mg(OH)_2$ nanoparticles on the thermal stability and flame retardancy of paraloid nanocomposites, J. Nanostruct. 4 (2014) 99–104.
[20] G. Nabiyouni, S. Sharifi, D. Ghanbari, M. Salavati-Niasari, A simple precipitation method for synthesis $CoFe_2O_4$ nanoparticles, J. Nanostruct. 4 (2014) 317–323.
[21] M. Panahi-Kalamuei, M. Mousavi-Kamazani, M. Salavati-Niasari, Facile hydrothermal synthesis of tellurium nanostructures for solar cells, J. Nanostruct. 4 (2014) 459–465.
[22] F. Beshkar, M. Salavati-Niasari, Facile synthesis of nickel chromite nanostructures by hydrothermal route for photocatalytic degradation of acid black 1 under visible light, J. Nanostruct. 4 (2015) 17–23.
[23] L. Nejati-Moghadam, A. Esmaeili Bafghi-Karimabad, M. Salavati-Niasari, H. Safardoust, Synthesis and characterization of SnO_2 nanostructures prepared by a facile precipitation method, J. Nanostruct. 4 (2015) 47–53.